High resolution study of the ν_2 and ν_5 rovibrational fundamental bands of thionyl chloride: Interplay of an evolutionary algorithm and a line-by-line analysis

Anthony Roucou,[1] Guillaume Dhont,[1] Arnaud Cuisset,[1,a)] Marie-Aline Martin-Drumel,[2] Sven Thorwirth,[3] Daniele Fontanari,[1] and W. Leo Meerts[4]
[1]*Laboratoire de Physico-Chimie de l'Atmosphère, CNRS EA-4493, Université du Littoral Côte d'Opale, 59140 Dunkerque, France*
[2]*Institut des Sciences Moléculaires d'Orsay, CNRS, Bâtiment 210, Université Paris-Saclay, 91405 Orsay Cedex, France*
[3]*I. Physikalisches Institut, Universität zu Köln, Köln, Germany*
[4]*Institute for Molecules and Materials, Molecular and Biophysics Group, Felix Laboratory, Radboud University, Toernooiveld 7c, 6525 ED Nijmegen, The Netherlands*

(Received 9 April 2017; accepted 18 July 2017; published online 3 August 2017)

The ν_2 and ν_5 fundamental bands of thionyl chloride ($SOCl_2$) were measured in the 420 cm^{-1} –550 cm^{-1} region using the FT-far-IR spectrometer exploiting synchrotron radiation on the AILES beamline at SOLEIL. A straightforward line-by-line analysis is complicated by the high congestion of the spectrum due to both the high density of $SOCl_2$ rovibrational bands and the presence of the ν_2 fundamental band of sulfur dioxide produced by hydrolysis of $SOCl_2$ with residual water. To overcome this difficulty, our assignment procedure for the main isotopologues $^{32}S^{16}O^{35}Cl_2$ and $^{32}S^{16}O^{35}Cl^{37}Cl$ alternates between a direct fit of the spectrum, via a global optimization technique, and a traditional line-by-line analysis. The global optimization, based on an evolutionary algorithm, produces rotational constants and band centers that serve as useful starting values for the subsequent spectroscopic analysis. This work helped to identify the pure rotational submillimeter spectrum of $^{32}S^{16}O^{35}Cl_2$ in the $v_2 = 1$ and $v_5 = 1$ vibrational states of Martin-Drumel *et al.* [J. Chem. Phys. **144**, 084305 (2016)]. As a by-product, the rotational transitions of the $v_4 = 1$ far-IR inactive state were identified in the submillimeter spectrum. A global fit gathering all the microwave, submillimeter, and far-IR data of thionyl chloride has been performed, showing that no major perturbation of rovibrational energy levels occurs for the main isotopologue of the molecule. *Published by AIP Publishing.* [http://dx.doi.org/10.1063/1.4996655]

I. INTRODUCTION

Thionyl chloride, $SOCl_2$, is an important reaction intermediate used by industries for manufacturing agrochemicals, dyestuffs, fine chemicals, and pharmaceuticals. It is an extremely powerful oxidant, and one of its primary uses is in the conversion of alcohols and carboxylic acids into their corresponding chlorides.[1] $SOCl_2$ has gained importance in the last quarter century due to its cathode role in lithium batteries and its global production exceeds 45 kt/year.[2] $SOCl_2$ is toxic and is listed as a Schedule 3 compound in the US Controlled Substances Act as it may be used for the production of chemical weapons. The atmospheric fate of $SOCl_2$ has been investigated by Johnson *et al.*[1] in a mixing chamber for various temperatures and relative humidity using Fourier transform (FT) infrared (IR) spectroscopy at low resolution. It was determined that humidity plays an important role, as water reacts rapidly with the parent compound, forming HCl and SO_2 in a nearly stoichiometric ratio of 2:1. Kinetic measurements demonstrated that the tropospheric lifetime due to hydrolysis is on the order of few minutes only. Taking into account several characteristics of $SOCl_2$ in terms of strong toxicity, violent reactivity, and rather large volatility, it is now established that improper disposal of $SOCl_2$ may have a significant pollution effect indoors and outdoors and the development of rapid, sensitive, and selective instrumentation is required to monitor $SOCl_2$ exhausted emissions. Over the last years, different types of toxic gas detectors have been developed with very good sensitivity (<1 ppb), even though they still suffer from selectivity.[3] To address this issue of selectivity, the next generation of toxic gas sensors will most likely probe molecule-specific rotational or rovibrational transitions.[4] A deep knowledge of thionyl chloride THz spectrum is thus mandatory to define ideal spectral windows and sensitivity thresholds for the development of such sensors.

From a spectroscopic point of view, $SOCl_2$ is a relatively heavy molecule, isotopically rich in natural abundance, and characterized as a highly asymmetric rotor involving two dipole moment components along the two principal axes *b* and *c* which define the symmetry plane of the molecule. These combined factors explain the huge density of rotational and rovibrational energy levels populated at room temperature.

a)Electronic mail: arnaud.cuisset@univ-littoral.fr

With respect to prior gas phase spectroscopic investigation studies of $SOCl_2$, the VUV spectrum has been recorded[5] and the fundamental vibrations have been measured by IR and Raman spectroscopies[6] without any resolution of the rotational structure.

Our group recently initiated an intensive high-resolution spectroscopic study of $SOCl_2$ and its isotopologues from the microwave to the far-IR regions.[4,7] Chirped-pulse FT microwave spectroscopy in supersonic expansion combined with high-level *ab initio* quantum-chemical calculations allowed the determination of accurate spectroscopic parameters for the six most abundant isotopologues and the determination of a highly accurate semi-experimental equilibrium geometry of $SOCl_2$.[4] At room temperature, very congested submillimeter and far-IR spectra have been rotationally resolved using a frequency multiplier chain and a high-resolution synchrotron-based FT-IR interferometer, respectively. Pure rotational transitions of the three most abundant isotopologues ($SO^{35}Cl_2$, $SO^{35}Cl^{37}Cl$, $SO^{37}Cl_2$) in their ground vibrational state have been assigned in the submillimeter spectrum in Ref. 4. Reference 7 describes the rovibrational analysis of the two low-energy IR active SCl_2 wagging ν_3 mode (symmetric, or A') and rocking ν_6 mode (asymmetric, or A'') in the far-IR domain. Unlike the ν_3 and ν_6 bands, the lowest energy band ν_4 predicted at 193.816 cm^{-1} and associated with the SCl_2 deformation[7] is too weak to be observed in the far-IR region, and the determination of its rotational constants and centrifugal parameters requires one to probe pure rotational transitions in vibrationally excited states. The ν_2 symmetric (A') and ν_5 asymmetric (A'') SCl_2 stretching bands, which lie higher in frequency in the far-IR region, respectively, around 495 cm^{-1} and 446 cm^{-1}, remain unobserved at high resolution to date.[7] Preliminary synchrotron-based FT-far-IR experiments failed to provide exploitable results due to strong interference with the intense ν_2 bending rovibrational band of sulfur dioxide SO_2 produced by reaction of $SOCl_2$ with residual water in the multipass cell.

The standard line-by-line assignment of high-resolution spectra is mostly based on pattern recognition. This procedure is time consuming and limited to well-resolved spectra with limited overlap between the transitions. A recently developed alternative consists in directly maximizing the overlap between the experimental and theoretical spectra.[8,9] A fitness function is defined as a normalized scalar product between the two spectra; the global maximum of this function corresponds to the best agreement between the two spectra.[10] The assignment problem is thus set up as a global optimization procedure where the spectroscopic parameters are tuned to maximize the fitness function. The main advantage of this approach is that it can automatically find the global maximum without assignment of rotational quantum numbers to individual transitions. In these last years, global optimization procedures based on evolutionary algorithms (EAs) have been used by some research groups to simplify the analyses of rotationally resolved electronic spectra on a large variety of molecular compounds such as floppy biomolecules[11] or atmospheric radicals.[12] It has recently been successfully applied to the analysis of a rovibrational spectrum of trimethylene sulfide collected with the FTIR instrument coupled to the far-IR beamline of the Canadian Light Source.[13]

Figure 1 shows the spectrum of $SOCl_2$ between 420 cm^{-1} and 550 cm^{-1} measured in this work at $P = 900$ μbars using the AILES beamline at SOLEIL.[14] It consists of the ν_2 and ν_5 bands of $SOCl_2$ and the ν_2 band of SO_2. The two bands have been analyzed for the two most abundant isotopologues $^{32}S^{16}O^{35}Cl_2$ and $^{32}S^{16}O^{35}Cl^{37}Cl$, referred to as [35, 35] and [35, 37] in the following, despite the strong overlap with the ν_2 band of SO_2. Each spectroscopic analysis requires an interplay between a global optimization, where the rotational constants and band center of the excited states for the two considered isotopologues are fitted, and a refinement of all the spectroscopic parameters via a line-by-line analysis using Loomis-Wood diagrams.[15]

In the following, Sec. II discusses the experimental setup that was used to record the far-IR spectrum. Section III presents the analyses that were performed on the ν_2 and ν_5 bands of the [35, 35] and [35, 37] isotopologues. This work also allowed a deeper investigation of the submillimeter/THz spectrum of Ref. 4. The pure rotational spectra of $SOCl_2$ in the $v_2 = 1$, $v_4 = 1$, and $v_5 = 1$ vibrational states are described in Sec. IV. Section V deals with a global fit of thionyl chloride, where both previous data[4,7,16–20] and the new assignments introduced in the present paper have been included. Section VI compares

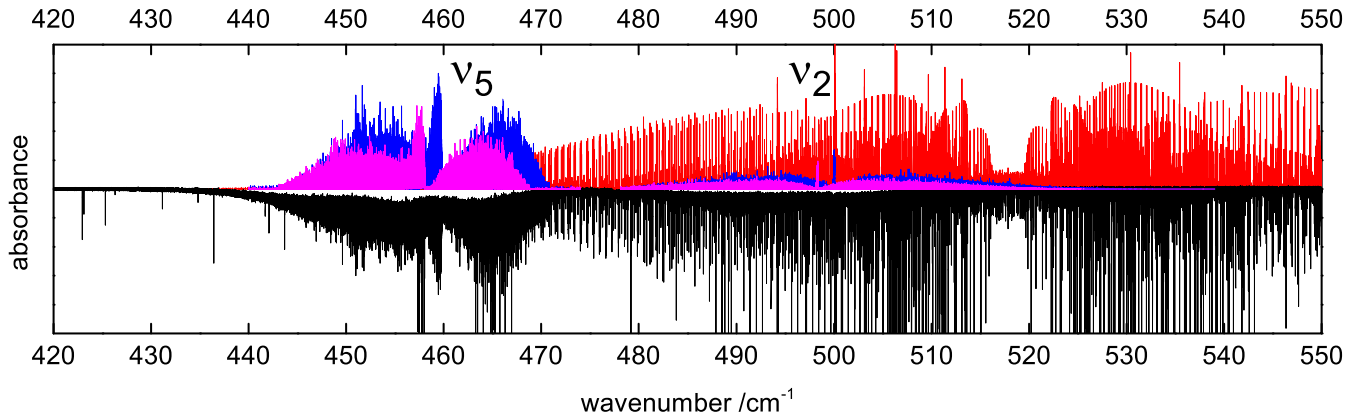

FIG. 1. Black: Experimental spectrum of $SOCl_2$. Red: Simulated spectrum of the ν_2 band of the SO_2 molecule. Calculated spectra of the ν_2 and ν_5 bands for the [35, 35] isotopologue (blue) and [35, 37] isotopologue (pink).

the results obtained from the procedure based on evolutionary algorithms with CCSD(T) *ab initio* calculations.

II. EXPERIMENT

The far-IR FT spectrum of thionyl chloride was collected on the AILES beamline of the SOLEIL synchrotron facility.[14] We chose an experimental configuration used previously for the high-resolution study of the ν_6 and ν_3 bands.[4,7] The synchrotron radiation was extracted and focused onto the entrance aperture of the Bruker IFS 125 FT interferometer equipped with a 6 μm mylar-silicon composite beamsplitter suitable for the THz/far-IR spectral range. The total absorption path length is greatly increased by using a White-type multipass cell adjusted to a 150 m optical path length and isolated from the interferometer by 50 μm-thick polypropylene windows. A helium-cooled silicon bolometer equipped with an optical band-pass filter in the range 10–700 cm^{-1} has been used to record the absorption spectrum. In the 420 cm^{-1}–550 cm^{-1} region, the synchrotron source provides a gain in the signal-to-noise ratio of 3 to 3.5 in comparison with a classical IR source (Hg lamp).[14] The acquisition time is therefore reduced by one order of magnitude. The present spectrum was recorded in 8 hours at 293 K by co-adding 100 interferograms recorded at the maximum resolution of the instrument (R = 0.001 02 cm^{-1}). The far-IR rovibrational linewidths are mainly limited by the apparatus function of the interferometer measured by Jacquemart *et al.*[21] to be approximately 100 MHz (FWHM). At 293 K, the far-IR Doppler linewidth never exceeds 20 MHz (FWHM).

The interferometer was continuously evacuated to 10^{-3} Pa limiting the absorption of atmospheric water. $SOCl_2$, of stated purity higher than 97% from Sigma-Aldrich,[22] was used without further purification. Its equilibrium vapor pressure at room temperature was injected directly into the absorption cell. The very efficient hydrolysis of $SOCl_2$ with gas traces of water produced a strong SO_2 band in the spectral region recorded. This band corresponds to the ν_2 bending mode centered at 513.539 cm^{-1} of the SO_2 molecule.[23] Its *P* branch is largely mixed with the ν_2 band of the $SOCl_2$ molecule centered at 500.094 cm^{-1} (SCl symmetric stretching mode) and with the *R* branch of the ν_5 band centered at 459.821 cm^{-1} (ClSCl asymmetric stretching mode). To reduce the gas traces of water and thus to reduce the presence of the SO_2 band, the cell was carefully pumped out before the experiment. The spectrum in Fig. 1 was calibrated using residual water absorption lines whose wavenumbers were taken from Refs. 24 and 25. The experimental error was estimated at 0.000 15 cm^{-1} taking into account the average $\tilde{\nu}_{obs} - \tilde{\nu}_{ref}$ from the calibration with water lines.

III. ANALYSIS OF THE ν_2 AND ν_5 ROVIBRATIONAL BANDS OF $SOCl_2$

A. Evolutionary algorithms

The painful study of high-resolution congested spectra has recently been alleviated with the use of EAs in spectroscopy.[10] The traditional assignment problem, which requires a time-consuming line-by-line analysis, is replaced by an algorithm maximizing the overlap between the simulated and experimental spectra. The frequency and intensity information of each spectrum is encoded in an *n*-dimensional vector (with *n* the number of experimental points). A fitness function *F* is introduced,[8] which is the normalized scalar product between the vectors **f** and **g**, representing, respectively, the experimental and calculated spectra. The scalar product is weighted by a symmetric matrix *W*, see Eq. (1). The matrix *W* permits more flexibility in the comparison between the calculated and experimental spectra. Additional details can be found in the Ref. 8,

$$F(\mathbf{f},\mathbf{g}) = \frac{\mathbf{f}^T W \mathbf{g}}{\sqrt{\mathbf{f}^T W \mathbf{f}}\sqrt{\mathbf{g}^T W \mathbf{g}}}. \quad (1)$$

Section II.C. of Ref. 10 discussed the choice of the fitness function and concluded that Eq. (1) was more suitable than a sum of square differences because spectra with nearly identical sets of parameters could be more easily distinguished with the former function. Maximizing the agreement between the experimental and calculated spectra translates to maximizing the fitness function. The best set of parameters is given by the global maximum of the fitness function. Among the techniques of global optimization, we chose EAs which are global optimizers based on concepts copied from the theory of evolution. Each spectroscopic parameter is represented as a gene, and a set of spectroscopic parameters (i.e., the rotational constants, the band centers, and the centrifugal distortion parameters) constitutes a chromosome. From each chromosome, one can compute a theoretical spectrum **g**. In a first step, the parameters are randomly generated in a range of chosen values. Second, the parameters are adjusted in the evolution phase using concepts derived from genetics such as inheritance, mutation, and crossover. For a given generation, the fitness function is computed for all the chromosomes and only the chromosomes giving the best results are kept in the next generation (selection). New chromosomes are built from the previous ones by mutating and crossing the values of their genes (spectroscopic parameters).

The global optimization is performed via the covariance matrix adaptation evolutionary strategy (CMA-ES),[26,27] which is an improved sibling of the genetic algorithms. The basic genetic algorithms are inefficient because they sample the parameter space randomly. The efficiency of the CMA-ES method is that it uses the information given by the evaluation of the fitness function for the chromosomes to move faster in the directions where the fitness function increases. The main advantage of the EA procedure over a more traditional fitting by, for example, the Levenberg-Marquardt (LM) algorithm is the fact that the EA performs a global search over the parameter space. Even until convergence is reached the EA will still consider the full parameter space. The needed computing time is fully determined by the number of calls to the model to calculate the spectrum, and this is comparable for the EA and the LM algorithms.

The two ν_5 and ν_2 bands of the spectrum in Fig. 1 were analyzed by means of the EA program[9,10,28] by considering the two most abundant isotopologues, [35, 35] (natural abundance: 54.45%) and [35, 37] (34.82%).

B. Analysis of the ν_5 band

1. Band center and rotational constants of the [35, 35] isotopologue

Initially, the spectra were prepared for application of the EA program by removing portions of the spectrum around frequency ranges containing H_2O lines[24,25] and the very congested Q branches. To better see the local features of the spectrum, a smoothed background was computed from the experimental spectrum by locally averaging over the neighbouring frequencies, and this background was subtracted to both experimental and simulated spectra. The experimental transitions of the ν_5 band were fitted using an effective Hamiltonian of Watson (type A, representation I^r) suited for an asymmetric rotor. The band center and the rotational constants of the $\upsilon_5 = 1$ excited state of both isotopologues were then optimized by using the EA program up to $J = 75$. The experimental ground state parameters were taken from previous microwave/far-IR analysis[4] and kept fixed. The distortion parameters of the $\upsilon_5 = 1$ state were kept fixed at the values of the ground vibrational state.

Each of the parameters to be fitted via an evolutionary algorithm must be given a range within which the experimental value is supposed to be found. In particular, a rather good estimation of the rotational constants for the excited vibrational states of [35, 35] is obtained by scaling the ground state experimental constants $[A, B, C]^{G.S.}_{\text{exp.}}$ of [35, 35] with the $\mathcal{F}^{ab\ initio}_{\text{scaling}}$ factor, ratio of the *ab initio* rotational constants of the ground and excited states,[7] see Eq. (2). The *ab initio* calculated values were computed at the MP2 level with a 6-311++G(3df,3pd) basis.[7] The Møller-Plesset (MP) second-order perturbed method with such a basis set provides a good compromise between accuracy and computation costs for the theoretical determination of rotational constants, and harmonic and anharmonic frequencies for medium size molecules,

$$[A, B, C]^{(\upsilon)}_{\text{est.}} = [A, B, C]^{G.S.}_{\text{exp.}} \times \mathcal{F}^{ab\ initio}_{\text{scaling}} \text{ with}$$
$$\mathcal{F}^{ab\ initio}_{\text{scaling}} = \frac{[A, B, C]^{(\upsilon)}_{ab\ initio}([35, 35])}{[A, B, C]^{G.S.}_{ab\ initio}([35, 35])}. \quad (2)$$

Since the spectra of [35, 37] are only 64% of the strength of the [35, 35] spectra, it was necessary to include the [35, 37] spectrum in the EA and to release the corresponding parameters along with those of the [35, 35]. A first guess of the rotational constants for the excited vibrational states of [35, 37] was obtained by scaling the ground state experimental constants $[A, B, C]^{G.S.}_{\text{exp.}}$ of [35, 37] with the same $\mathcal{F}^{ab\ initio}_{\text{scaling}}$ factor as used for [35, 35], see Eq. (2).

At the first generation, the EA procedure randomly selects the parameters in the range given as input. These ranges were centered on the estimated values $[A, B, C]^{(\upsilon)}_{\text{est.}}$ of [35, 35] and [35, 37], and the full widths were empirically found (60 MHz for A, 30 MHz for B and C). As it was more difficult to find a good range for the band center, we have cut a large frequency interval around the Q branch (3 cm^{-1}) into smaller chunks (0.3 cm^{-1}) and performed a global optimization on each chunk. A good determination of the rotational constants and band center was obtained for [35, 35] after 5 h of calculation.[29] The correctness of the parameters in the chromosome associated with the best fitness function was established by an eye comparison between the calculated spectrum derived from these parameters and the experimental spectrum.

Some trials to fit directly via a global optimization the complete effective Hamiltonian, i.e., with optimizing the distortion terms too, have been attempted but did not converge towards a satisfactory set of parameters. This can be explained by several factors: a congested spectrum due to the two isotopologues, and the complicated landscape of the fitness function due to the multidimensional space and the large number of local maxima.

2. Subsequent standard spectroscopic analysis of the [35, 35] isotopologue

The parameters associated with the excited $\nu_5 = 1$ state of the [35, 35] isotopologue were released (i.e., the band center and rotational constants as in the EA procedure but quartic and sextic centrifugal distortion terms as well) and the transitions were fitted by a traditional line by line analysis using the SPFIT/SPCAT suite of programs[30] with the help of Loomis-Wood diagrams.[15] These diagrams facilitate the visual identification of individual spectral branches in complicated spectra with overlapping bands and/or high density of lines. In a given branch, only the J quantum number changes by 1 along the series. The K_a and K_c values of the lower and upper states are fixed as determined by the selection rules. A Loomis-Wood diagram is obtained by cutting the spectrum in the neighborhood of the calculated transitions and pasting them one above the others for each J'' value of the branch. Consequently, the differences between the experimental transition frequencies with the calculated transition frequencies are represented horizontally for each J'' value of the branch. Ideally, a good assignment of the lines leads to symbols representing the experimental lines aligned vertically in the center of the Loomis-Wood diagram.

Examples of Loomis-Wood diagrams generated with the LWWa software[15,31] are given in Fig. 2, representing the evolution at each step of the analysis. Figures 2(a) and 2(b) show the Loomis-Wood diagrams for, respectively, the ${}^qP(3)$ and ${}^qR(3)$ branches with the estimated rotational constants from Eq. (2). Many series are distinguishable, but the good assignment, identified by the magenta and orange colours, respectively, is not obvious. Figures 2(c) and 2(d) give the diagram after the global optimization step using the EA program. The agreement is visible between the calculated and experimental transitions, but for high values of J'', the deviation of the peaks with respect to the centered vertical line calls for an improvement in the centrifugal distortion constants. Figures 2(e) and 2(f) are the diagrams with the final spectroscopic constants and demonstrate the importance of the refinement of the centrifugal distortion terms in the line by line analysis.

The standard spectroscopic analysis gives a definite set of experimental spectroscopic parameters for the main isotopologue, see Table I. We determined the centrifugal distortion constants up to the sextic order in power of J. The IR unitless standard deviation of 0.645 indicates that the experimental error of 0.000 15 cm^{-1} is slightly overestimated. The fitted molecular parameters reproduce nicely the ν_5 band of [35, 35].

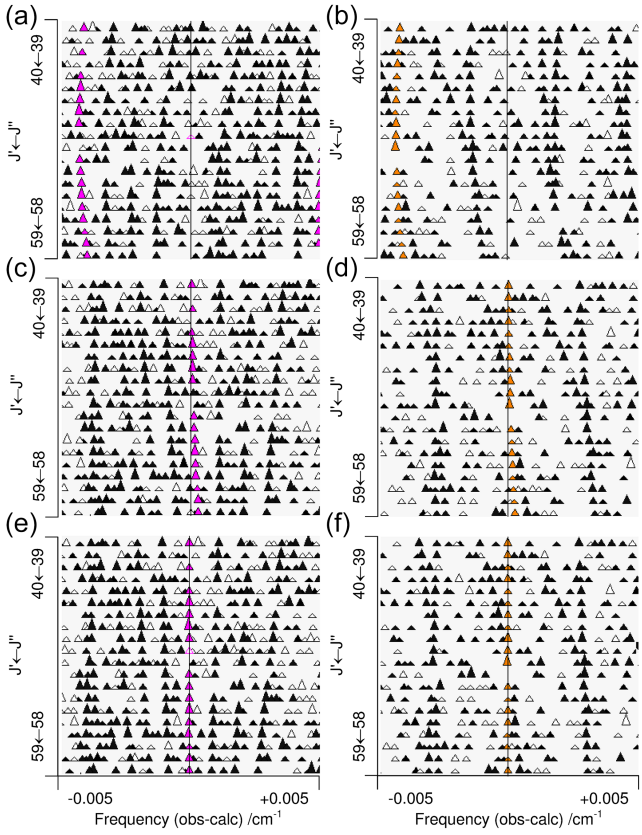

FIG. 2. Loomis-Wood diagrams of ${}^qP(3)$ (left column) and ${}^qR(3)$ (right column) branches for each step of the analysis of the main isotopologue [35, 35] of the ν_5 band. Black triangles correspond to the assigned transitions of [35, 35] and the empty triangles correspond to unassigned transitions. (a) and (b) show the Loomis-Wood diagrams with the initial estimated rotational constants [from Eq. (2)] for, respectively, the ${}^qP(3)$ (magenta triangles) and ${}^qR(3)$ (orange triangles) branches. (c) and (d) give the diagrams after the global optimization step. (e) and (f) are the diagrams with the experimental spectroscopic constants after the refinement of the centrifugal distortion terms in the line by line analysis.

The resulting calculated spectrum for [35, 35] compared with the experimental ν_5 band is given in Fig. 3. In particular, the patterns in each branch (P, Q, R) are reproduced.

The relative accuracy of the predicted band centers and rotational constants has been quantified using a δ parameter defined by

$$\delta = \frac{|\text{experimental} - \text{calculated}|}{\text{experimental}}.$$

The relative accuracy values follow each step of the analysis: estimated value from Eq. (2), refined value from Eq. (3), observed (from the maximal intensity of the Q branch in the experimental spectrum), and EA.

The relative accuracy of the predictions for the band centers and rotational constants has been estimated at each step of the analysis, and their evolutions are shown in Figs. 4(a) and 4(e), respectively. For the rotational constants, the EAs achieved a relative accuracy better than 10^{-4} while initial *ab initio* values at the MP2/6-311++G(3df,3pd) level of theory were close to 1%. The efficiency of EAs is also remarkable for the estimation of the rovibrational band centers with a reduction by 3 orders of magnitude compared to the initial *ab initio* values: relative accuracy of 3×10^{-6} is reached for the ν_5 band center.

TABLE I. Summary of the fitted parameters in the far-IR analysis of the ν_5 band for the two isotopologues [35, 35] and [35, 37]. 1σ uncertainties[32] are quoted in parentheses in the unit of the last digit. Below are given the number N of different experimental lines in the fit, maximum values of quantum number $J''_{\max}$ and associated $K''_{a\,\max}$ value, and the standard deviation. The unitless standard deviation of a set of N calculated frequency transitions $f_i^{\text{calc.}}$ compared to a set of experimental frequency transitions $f_i^{\text{obs.}}$ measured with experimental errors Δ_i is defined as $\sqrt{\frac{1}{N}\sum_i \left(\frac{f_i^{\text{obs.}} - f_i^{\text{calc.}}}{\Delta_i}\right)^2}$. All parameters (except band centers and standard deviation) are given in MHz.

	ν_5	
	[35, 35]	[35, 37]
ν	13 785 076.733(166)	13 732 558.918(193)
ν (cm^{-1})	459.820 664 8(55)	458.068 859 0(64)
A	5 072.604 85(149)	5 030.389 9(107)
B	2 809.808 63(48)	2 736.642 41(225)
C	1 952.108 147(177)	1 910.689 111(106)
$D_J \times 10^3$	1.107 866(125)	1.113 10(116)
$D_{JK} \times 10^3$	−2.274 28(99)	−4.503(41)
$D_K \times 10^3$	7.049 2(32)	13.481(116)
$\delta_J \times 10^3$	0.392 099(67)	0.399 37(58)
$\delta_K \times 10^3$	1.376 09(52)	0.454 9(162)
$\Phi_J \times 10^9$	0.329 8(188)	
$\Phi_{JJK} \times 10^6$	0.007 092(153)	
$\Phi_{JKK} \times 10^6$	−0.044 37(74)	
$\Phi_K \times 10^6$	0.054 22(189)	
$\phi_J \times 10^9$	0.203 8(96)	
$\phi_{JK} \times 10^9$	2.927(94)	
$\phi_K \times 10^6$	0.023 14(45)	
N	292 5	153 2
$J''_{\max}$	114	125
$K''_{a\,\max}$	37	17
Standard deviation IR (cm^{-1})	0.000 10	0.000 14
Unitless standard deviation IR	0.645	0.938

3. Band center and rotational constants of the [35, 37] isotopologue

A second global optimization procedure of the band center and rotational constants was performed for the [35, 37] isotopologue. Here, all the parameters associated with the excited state of the main [35, 35] isotopologue are now frozen to the values obtained at the end of the standard spectroscopic analysis of that species. The guessed rotational constants for [35, 37] are refined by scaling the ground state experimental constants $[A, B, C]^{G.S.}_{\text{exp.}}$ of [35, 37] with the $\mathcal{F}^{exp.}_{\text{scaling}}$ factor, ratio of the experimental rotational constants of the ground and excited states of [35, 35], see Eq. (3):

$$[A, B, C]^{(v)}_{\text{refined}}\,[35, 37] = [A, B, C]^{G.S.}_{\text{exp.}}\,[35, 37] \times \mathcal{F}^{exp.}_{\text{scaling}},$$
$$\text{with } \mathcal{F}^{exp.}_{\text{scaling}} = \frac{[A, B, C]^{(v)}_{\text{exp.}}([35, 35])}{[A, B, C]^{G.S.}_{\text{exp.}}([35, 35])}. \quad (3)$$

The range of the band center for [35, 37] was again found by dividing the range of permitted values around the Q branch (0.8 cm^{-1}) in smaller chunks (0.04 cm^{-1}). We selected the chromosome giving the best fitness among all the chunks and

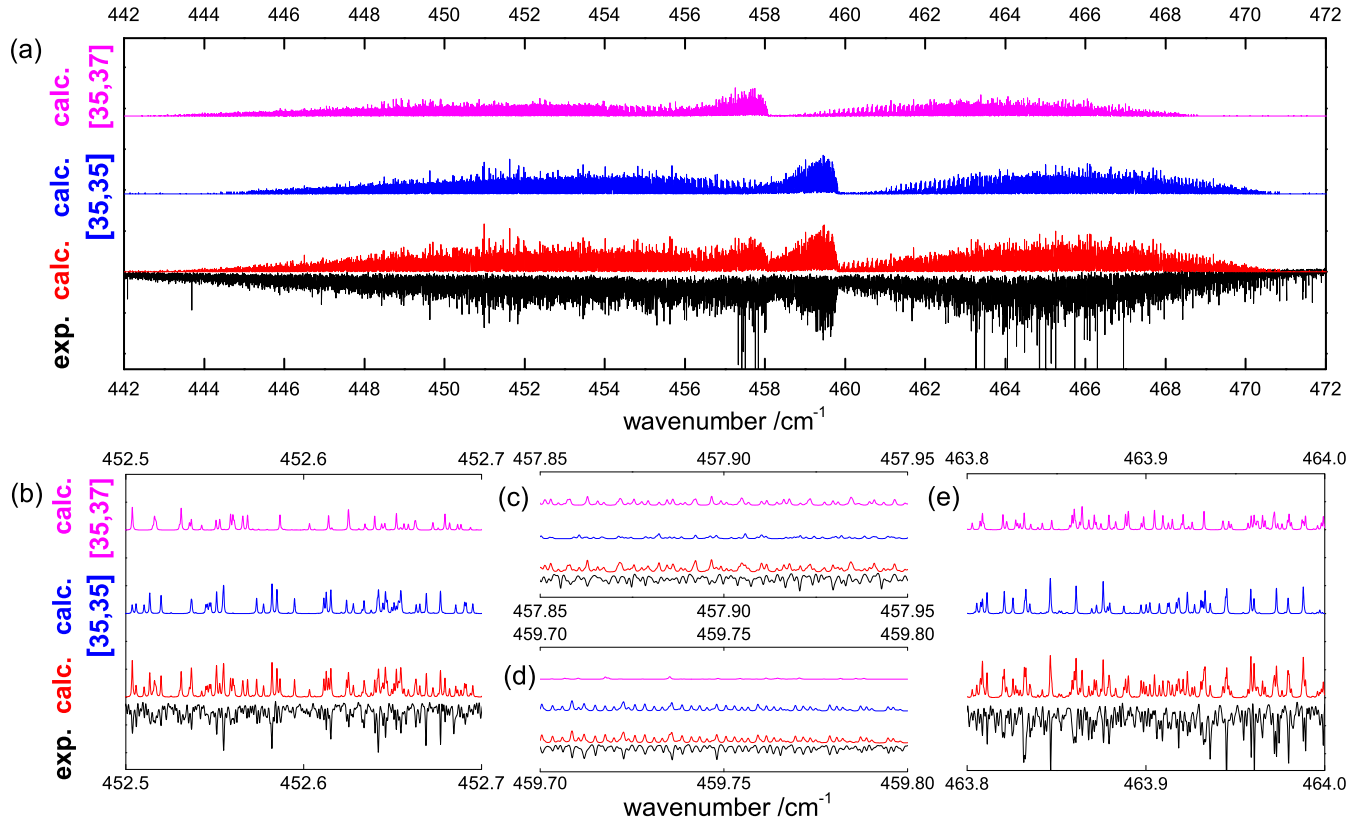

FIG. 3. (a) Experimental (black) and calculated spectra of ν_5 band for the two most abundant isotopologues [35, 35] (blue) and [35, 37] (pink). The red spectrum is the global synthetic simulated spectrum for the two isotopologues. (b) Part of the *P* branch. (c) Part of the *Q* branch for [35, 37]. (d) Part of the *Q* branch for [35, 35]. (e) Part of the *R* branch.

checked by visual comparison the agreement between the calculated and experimental spectra. A good determination of the rotational constants and band center was obtained for [35, 37] after 10 h of calculation.[29] For the same reason as the [35, 35] isotopologue, the distortion parameters of [35, 37] in the vibrational excited state have been kept frozen to the values of the corresponding ground state.

4. Subsequent standard spectroscopic analysis of the [35, 37] isotopologue

The band center and the rotational constants for the $v_5 = 1$ state of the [35, 37] isotopologue obtained at the end of the global optimization procedure were once more fitted against the experimental data, and the centrifugal distortion terms are now released as well. The definitive set of experimental spectroscopic parameters are given in Table I. Although we determined the centrifugal distortion constants up to sextic order in power of J for the [35, 35] isotopologue, we determined the centrifugal distortion terms up to the quartic order for the [35, 37] isotopologue because it was not possible to detect rovibrational transitions involving energy levels with sufficiently high K_a values ($K''_{a\,\max} = 17$). The far-IR standard deviation is very close to the experimental error which implies that the spectrum is fitted at the experimental precision, as implied by the unitless RMS of 0.938 very close to 1. The resulting calculated spectrum for [35, 37] compared with the experimental ν_5 band is given in Fig. 3. We note that all the patterns are reproduced in the simulated spectrum. Almost all the lines of the experimental spectrum are reproduced.

The evolution of the relative accuracy δ of the rovibrational band center and rotational constants can be found in Figs. 4(c) and 4(e). As for the [35, 35] isotopologue, the correspondence between the numerical values obtained after the EAs and the final experimental ones highlights the effectiveness of the EAs.

C. Analysis of the ν_2 band

The procedure to analyze the ν_2 band follows very closely the footsteps of the ν_5 analysis. The experimental spectrum was cleaned by removing the strongest SO_2 lines (simulated from molecular constants fitted in Ref. 23) and several H_2O lines[24,25] but the weaker transitions of SO_2 were still present and mixed with the $SOCl_2$ lines. In addition, the congestion and the weak intensity of the rovibrational lines of ν_2 resulted in a more difficult analysis compared to the ν_5 band. As more lines are blended and many lines are close to the noise amplitude, more local maxima in the fitness function hypersurface make the localization of the global maximum tricky. Moreover, by removing parts of the spectrum containing strong SO_2 lines, many overlapped $SOCl_2$ lines have also been removed. For these reasons, the initial ranges of the rotational constants were chosen narrower than for the ν_5 band (18 MHz for A, B and C), and the experimental transitions were fitted to the asymmetric rotor Hamiltonian up to $J = 80$. For [35, 35] and [35, 37], the Q

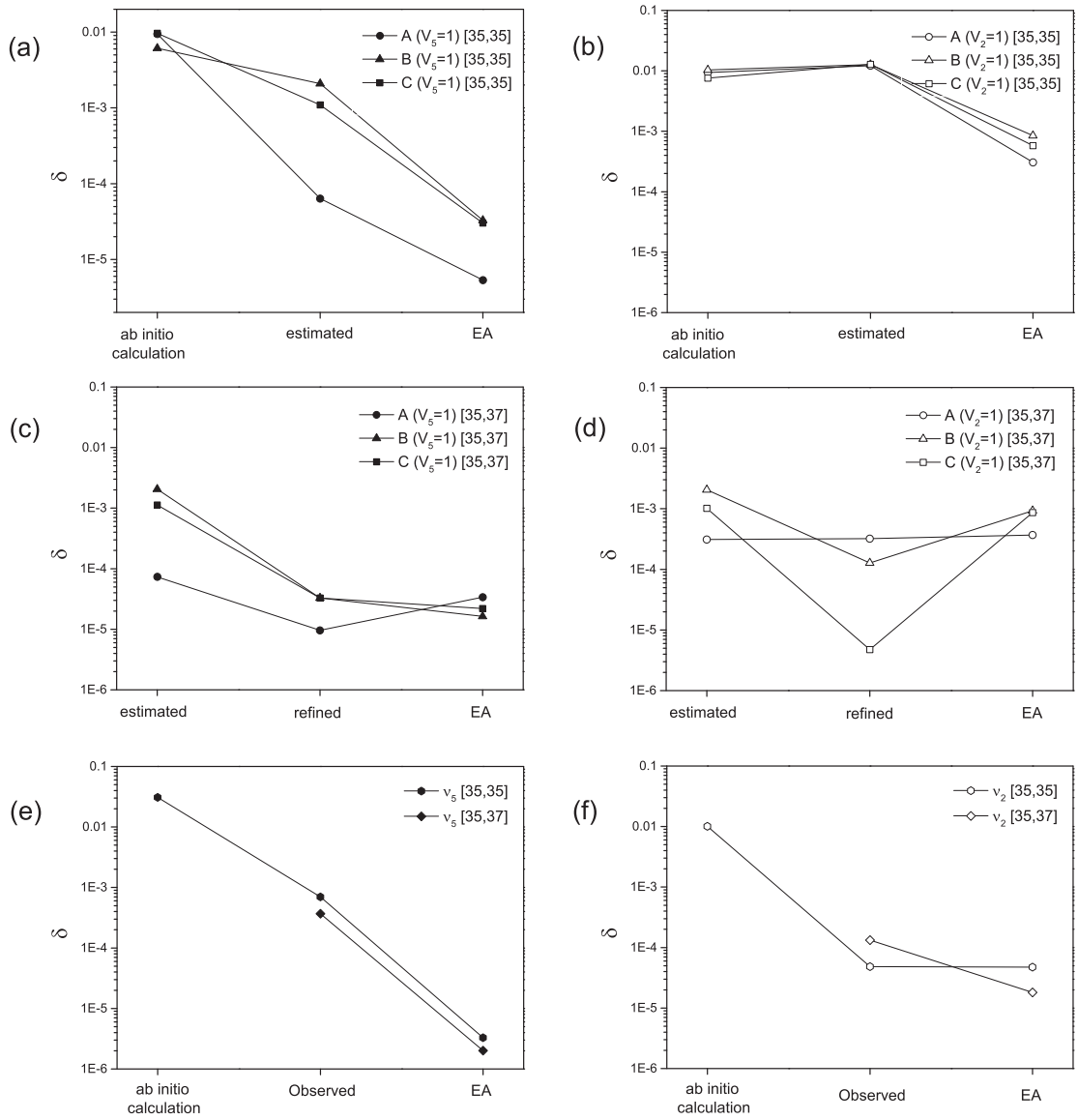

FIG. 4. Evolution in the log scale of the relative accuracy δ = |experimental − calculated| /experimental at each step of the analysis: *ab initio* calculation [at the MP2/6-311++G(3df,3pd) level of theory], estimated value from Eq. (2), refined value from Eq. (3), observed (from the maximal intensity of the Q branch in the experimental spectrum), and EA. δ is calculated for each EA optimized parameter: A, B, C rotational constants and rovibrational band centers. (a) The rotational constants of [35, 35] of $\upsilon_5 = 1$, (b) the rotational constants of [35, 35] of $\upsilon_2 = 1$, (c) the rotational constants of [35, 37] of $\upsilon_5 = 1$, (d) the rotational constants of [35, 37] of $\upsilon_2 = 1$, (e) the band center of the two isotopologues of $\upsilon_5 = 1$, and (f) the band center of the two isotopologues of $\upsilon_2 = 1$.

branches were narrow and the initial range of permitted values for the band center (0.2 cm^{-1}) was not divided in chunks. The calculation time was only 148 and 142 min,[29] respectively, for the [35, 35] and [35, 37] isotopologues.

Figure 4 shows the evolution along the spectroscopic analysis of the relative accuracy δ for the rotational constants and rovibrational band centers of the ν_2 fundamental band of [35, 35] and [35, 37]. For the rotational constants of [35, 35], the convergence towards the experimental value is nearly monotonic [Fig. 4(b)]. For [35, 37], the rotational constants [see Fig. 4(d)] obtained from the EA were not employed; instead we used the refined parameters $[A, B, C]^{(\upsilon_2=1)}_{\text{refined}}$ from Eq. (3). We noticed that the evaluation of the fitness function with the final experimental parameters of [35, 37] is slightly lower than the best value of the fitness function given by the global optimization (search of a global maximum) of the EA procedure. This problem can be explained by our use of two complementary methods: the line by line spectroscopic analysis of [35, 37] only uses clearly defined lines of this isotopologue while the global optimization uses the experimental spectrum with the possible existence of perturbed lines of the $SOCl_2$ isotopologues and the SO_2 molecule. In Fig. 4(f), the values of the band centers obtained after the EA step are very close to the experimental ones with relative δ values better than 10^{-4} whereas the relative accuracy of *ab initio* calculations are limited to 1%. It shows that the EA leads to a very good determination of all the band centers, crucial for good assignments with the Loomis-Wood diagrams. The final set of experimental spectroscopic parameters of [35, 35] and [35, 37] of the ν_2 band are summed up in Table II. The far-IR standard deviations are very close to the estimated experimental error. The centrifugal distortion constants were determined up to

TABLE II. Summary of the fitted parameters in the far-IR analysis of the ν_2 band. 1σ uncertainties[32] are quoted in parentheses in the unit of the last digit. Below are given the number N of different experimental lines in the fit, maximum values of quantum number J''_{max} and associated $K''_{a\,max}$ value, and the standard deviation. See the caption of Table I for the definition of the unitless standard deviation. All parameters (except band centers and standard deviation) are given in MHz.

	ν_2	
	[35, 35]	[35, 37]
ν	14 992 447.162(208)	14 940 637.482(298)
ν (cm^{-1})	500.094 207 2(69)	498.366 022 3(100)
A	5 083.311 7(90)	5 042.574 9(238)
B	2 823.404 04(212)	2 749.443 0(58)
C	1 959.369 498(167)	1 917.742 688(230)
$D_J \times 10^3$	1.038 85(79)	0.805 9(38)
$D_{JK} \times 10^3$	1.166 6(144)	2.417(75)
$D_K \times 10^3$	−0.724(52)	2.053(279)
$\delta_J \times 10^3$	0.344 77(40)	0.234 12(192)
$\delta_K \times 10^3$	2.399 6(65)	2.162(35)
N	142 9	854
J''_{max}	87	87
$K''_{a\,max}$	15	12
Standard deviation IR (cm^{-1})	0.000 13	0.000 14
Standard deviation IR unitless	0.856	0.940

quartic order for the two [35, 35] and [35, 37] isotopologues. It was not possible to reach the sextic order constants with an acceptable uncertainty in the parameters. Compared with the ν_5 band, the ν_2 band was more congested with less intense lines, and it was not possible to assign transitions with $J > 87$ and $K_a > 15$ (see Tables I and II). The simulated spectra of [35, 35] and [35, 37] are represented in Fig. 5 and compared with the experimental spectrum. The spectra present a good agreement, each pattern can be easily recognized, especially in the Q branches. The experimental ν_2 spectrum presents more remaining non-predicted weak lines than for the ν_5 band due to SO_2.

IV. SUBMILLIMETER SPECTRUM ANALYSIS

The new data gathered for the ν_2 and ν_5 bands allow the prediction of the pure rotational transitions in the $v_2 = 1$ and $v_5 = 1$ vibrational states. The experimental spectrum published in Ref. 4 is a room temperature absorption spectrum of $SOCl_2$ that has been probed in the submillimeter domain by the radiation generated from a frequency multiplier chain (Virginia Diodes, Inc.). All experimental details concerning the spectrometer and the experimental conditions have been reported previously in Refs. 33 and 4, respectively. The pure rotational transitions have been already assigned for the vibrational ground state of the three most abundant isotopologues [35, 35], [35, 37], and [37, 37] and for the vibrational excited states $v_3 = 1$ and $v_6 = 1$ of [35, 35].[4,7,16–20] Our paper completes the analysis by proposing an assignment for the pure rotational transitions of

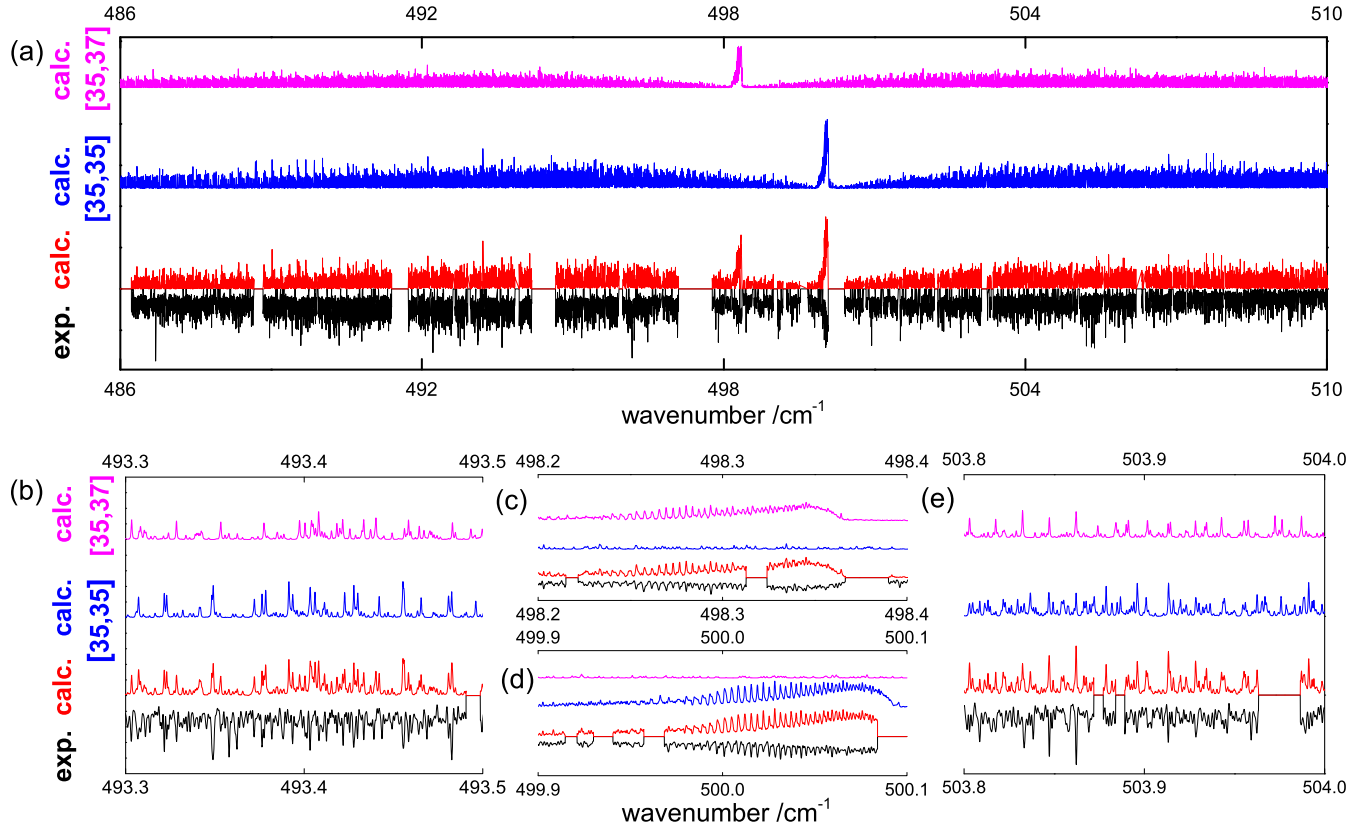

FIG. 5. (a) Experimental (black) and calculated spectra of the ν_2 band for the two most abundant isotopologues [35, 35] (blue) and [35, 37] (pink). The red spectrum is the global synthetic simulated spectrum for the two isotopologues. (b) Part of the P branch. (c) Part of the Q branch for [35, 37]. (d) Part of the Q branch for [35, 35]. (e) Part of the R branch. Some parts of the spectrum have been removed for the EA procedure because they contained strong SO_2 and H_2O lines.

TABLE III. Summary of the final fitted parameters in the rotational and rovibrational analyses of [35, 35]. 1σ uncertainties[32] are quoted in parentheses in the unit of the last digit. Below are given the number N of different experimental lines in the fit, maximum values of quantum number J''_{max} and associated $K''_{a\,max}$ value, and the standard deviation. See the caption of Table I for the definition of the unitless standard deviation. All parameters (except indicated otherwise) are given in MHz.

	ν_4	ν_5	ν_2
ν	[5 810 457.503]	13 785 076.908(114)	14 992 446.403(214)
ν (cm^{-1})	[193.816]	459.820 670 6(38)	500.094 181 9(71)
A	5 108.588 988(154)	5 072.603 864(181)	5 083.209 84(39)
B	2 814.471 870(78)	2 809.806 675(142)	2 823.426 43(32)
C	1 952.767 488(93)	1 952.107 746(127)	1 959.372 070(226)
$D_J \times 10^3$	1.117 762 7(148)	1.107 538 0(296)	1.060 820(66)
$D_{JK} \times 10^3$	−2.218 849(64)	−2.278 275(118)	0.928 374(224)
$D_K \times 10^3$	7.152 212(149)	7.059 216(126)	−0.843 020(307)
$\delta_J \times 10^3$	0.394 297 8(66)	0.391 992 2(143)	0.355 380(33)
$\delta_K \times 10^3$	1.314 005(64)	1.376 396(130)	2.361 660(301)
$\Phi_J \times 10^9$	0.400 72(99)	0.285 76(234)	8.088 6(59)
$\Phi_{JJK} \times 10^6$	0.006 384 2(104)	0.007 452 1(271)	−0.100 477(65)
$\Phi_{JKK} \times 10^6$	−0.044 976 8(287)	−0.048 894(79)	−0.045 991(191)
$\Phi_K \times 10^6$	0.064 268(61)	0.064 684(57)	0.016 573(138)
$\phi_J \times 10^9$	0.221 27(50)	0.185 48(123)	4.019 00(312)
$\phi_{JK} \times 10^9$	1.404 6(79)	3.257 1(195)	−18.391(50)
$\phi_K \times 10^6$	0.019 180 3(304)	0.023 082(92)	−0.044 366(220)
$L_K \times 10^{12}$	−0.239 9(70)		
N	5 172	5 442	2 091
J''_{max}	106	114	90
$K''_{a\,max}$	64	60	60
Standard deviation MW (MHz)	0.091 316	0.136 071	0.168 047
Standard deviation IR (cm^{-1})		0.000 10	0.000 13
Unitless standard deviation	0.913 16	0.954 80	1.089 82

the $v_2 = 1$, $v_5 = 1$ and $v_4 = 1$ vibrational excited states of the [35, 35] isotopologue. The ν_4 vibrational band is not IR-active; the $v_4 = 1$ state could only be analyzed in the submillimeter domain from pure rotational transitions induced by the permanent dipole moment and involving thermally populated levels in $v_4 = 1$. The analysis was performed with the AABS package from Kisiel[34,35] in parallel with SPFIT/SPCAT.[30] The rotational spectroscopic parameters together with a summary of the study for the $v_5 = 1$, $v_2 = 1$, and $v_4 = 1$ are given in Table III. Each contribution in the experimental spectrum is shown in Fig. 6(a). The comparison between experimental and calculated spectra is shown in Fig. 6(b) for two frequency ranges: 255-295 GHz (left) and 273.5-274.5 GHz (right). The $v_5 = 1$ and $v_2 = 1$ states are significantly higher in energy compared to $v_4 = 1$ and thus present weaker lines in the submillimeter domain. New rotational transitions have been assigned: 5172, 2517, and 662 lines for $v_4 = 1$, $v_5 = 1$, and $v_2 = 1$, respectively. Some of them are marked with triangles in the stick spectrum [Fig. 6(b)]. This analysis has permitted us to probe transitions with higher J and K_a values, thus improving the parameters obtained from the rovibrational analysis of $v_5 = 1$ and $v_2 = 1$ of [35, 35] (see Tables I and II). The far-IR standard deviations obtained in the rovibrational study were not deteriorated for the $v_5 = 1$ and $v_2 = 1$ states: for each of the states $v_5 = 1$, $v_2 = 1$, and $v_4 = 1$, the standard deviation from pure rotational lines ("standard deviation MW," see Table III) is in the range of the experimental error of 100 kHz, which is reflected by the dimensionless standard deviation very close to 1.

Because the Cl–S–Cl scissoring mode is barely far-IR active, no band center has been experimentally determined for $v_4 = 1$. Nevertheless, the submillimeter analysis of the pure rotation in the ν_4 excited state gave access to the rotational constants with a degree of precision similar to the other bands. Indeed, the ν_4 state is the lowest-energy vibrational mode of $SOCl_2$ with an estimated anharmonic frequency of 193.816 cm^{-1} at the MP2/6-311++G(3df,3pd) level of theory, and the intensity of the rotational lines is comparable to the ground state lines of the intensity of the [37, 37] isotopologue (see Fig. 6). Unlike the submillimeter assignments of vibrational satellites from the $v_6 = 1$ and $v_3 = 1$ states where the distortion constants were limited to sextic order, the octic order L_K term has been fitted for $v_4 = 1$. Finally, due to the weakness of the line intensities, it was not possible to assign rotational transitions in the vibrationally excited states for the less abundant isotopologues.

V. GLOBAL FIT FOR THE THIONYL CHLORIDE

A global fit for each isotopologue was performed that include the assignments of the previous analyses[4,7,16–20] and the new data measured in the present study. Table IV sums up the origin of the different data. The global fits include 38 910 and 15 258 experimental lines, with 104 and 54 fitted

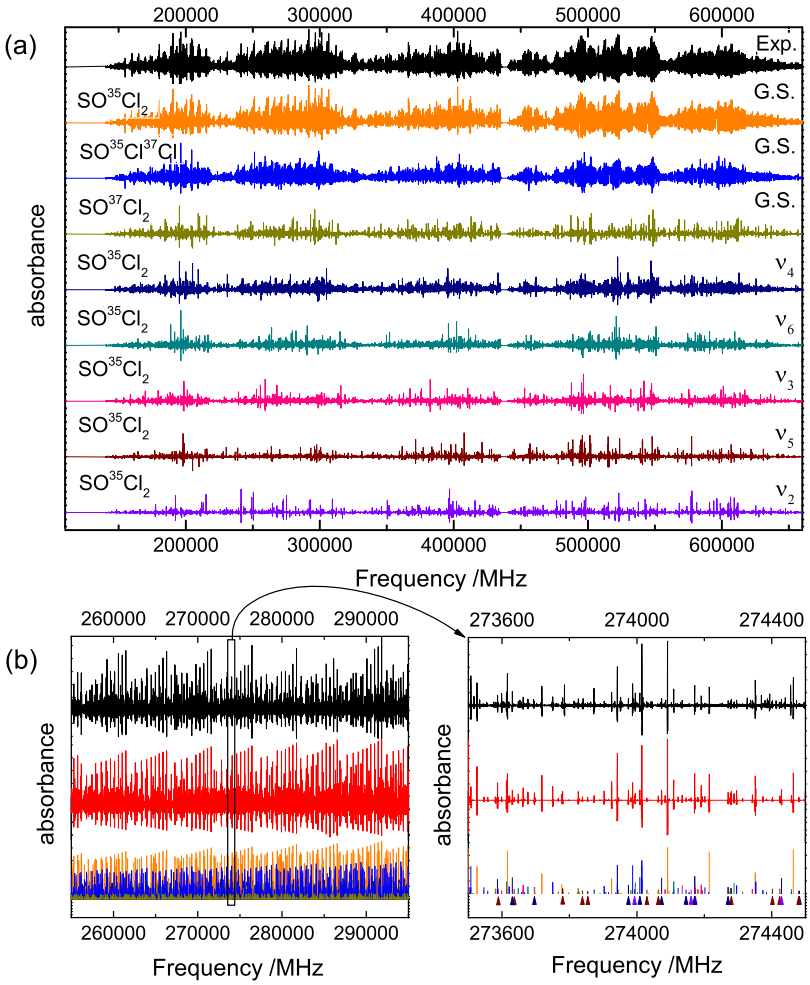

FIG. 6. (a) Experimental submillimeter spectrum of thionyl chloride (in black) and all the experimental individual contributions considered in the analysis. Note that the experimental output power varies with the multiplication stages [140-220 GHz (×18), 220-330 GHz (×27), 330-440 GHz (×36), 440-660 GHz (×54)]. (b) Comparison between the experimental spectrum (in black), the global synthetic simulation (in red), and the stick spectrum of the individual contributions [the colour of each contribution agrees with panel (a)]. The triangles on the 273.5-274.5 GHz stick spectrum mark the rotational lines newly assigned in this study.

parameters, respectively, for [35, 35] and [35, 37]. The parameters obtained from this fit can be found in Table V.

The combination of the different assignments in the global fit does not deteriorate the standard deviation of the fit and the accuracies of the fitted parameters compared to individual band analyses. In Fig. 7, the rovibrational energy levels from [35, 35] have been calculated up to $J = 80$ from the parameters of the five lowest energy fundamental vibrational bands (see Table V). The vibrational centers of two combination bands $\nu_4 + \nu_6$ and $2\nu_4$ calculated at the anharmonic MP2/6-311++G(3df,3pd) level of theory are indicated. For the fundamental bands, the solid lines represent the energy of the relative equilibria, i.e., the energy of the classical stationary axes of rotation.[36–38] Figure 7 shows that an overlap between the different bands starts to appear for $J > 20$. Nevertheless, all the experimental transitions could be fitted without consideration of any effective Coriolis or Fermi interactions between fundamental and combination bands. Indeed, the Loomis-Wood analysis used in the vibrationally excited rotational transition assignments never shows any signature of possible interaction. However, in Table V, we can immediately notice that the quartic and sextic distortion constants for all excited vibrational modes are very close to the ground state values except for the $v_2 = 1$ level where several distortion constants are quite different in value. It suggests that the SCl symmetric stretching vibration is more strongly coupled to the rotation compared to the other vibrational modes. The possibility of an interaction with an other state could not be totally excluded ($\nu_4 + \nu_6$ is the closest level to ν_2) but we did not find any evidence of this perturbation.

TABLE IV. Origin of the data used in the global fit.

Reference	[35, 35]	[35, 37]
19	G.S. ← G.S.	
20	G.S. ← G.S.	G.S. ← G.S.
17		G.S. ← G.S.
16		G.S. ← G.S.
18	G.S. ← G.S.	
7	ν_3 ← G.S., ν_6 ← G.S.	
4	G.S. ← G.S., ν_3 ← ν_3, ν_6 ← ν_6, ν_3 ← G.S., ν_6 ← G.S.	G.S. ← G.S., ν_3 ← G.S. ν_6 ← G.S.
This work	ν_2 ← ν_2, ν_5 ← ν_5, ν_4 ← ν_4, ν_2 ← G.S., ν_5 ← G.S.	ν_2 ← G.S., ν_5 ← G.S.

VI. PREDICTIVE POWER OF COUPLED-CLUSTER CALCULATIONS

All the *ab initio* calculations presented in this study have been performed at the MP2/6-311++G(3df,3pd) level of theory.

TABLE V. Summary of the fitted parameters in the global fit, number N of different experimental lines and standard deviation. 1σ uncertainties[32] are quoted in parentheses in the unit of the last digit. The values in square brackets have been kept fixed to the values of the ground state in the global fit.[4] See the caption of Table I for the definition of the unitless standard deviation. Values indicated by [4] have been kept fixed according to the *ab initio* values found in Ref. 4. All parameters (except indicated otherwise) are given in MHz. For the [35, 37] isotopologue, no experimental values of ν_4 are included because no assignment of the excited states of the submillimeter spectrum was possible.

	[35, 35]					
	GS	ν_4	ν_6	ν_3	ν_5	ν_2
ν		[5 810 457.503]	8 505 880.092(93)	10 371 817.238(93)	13 785 076.825(119)	14 992 446.406(195)
ν (cm^{-1})		[193.816]	283.7 619 7(31)	345.966 583 3(31)	459.820 667 8(40)	500.094 182 0(63)
A	5 086.748 253 8(117)	5 108.588 988(168)	5 074.500 612(147)	5 079.016 861(138)	5 072.603 762(188)	5 083.209 83(36)
B	2 822.530 070 7(108)	2 814.471 870(84)	2 826.464 556(83)	2 816.388 811(88)	2 809.806 700(147)	2 823.426 440(293)
C	1 960.313 909 2(89)	1 952.767 488(101)	1 959.792 902(84)	1 958.578 914(97)	1 952.107 813(133)	1 959.372 087(206)
$D_J \times 10^3$	1.125 141 1(35)	1.117 762 7(161)	1.134 571 6(148)	1.125 066 6(173)	1.107 544 1(309)	1.060 820(60)
$D_{JK} \times 10^3$	−2.226 751 8(265)	−2.218 849(70)	−2.199 020(73)	−2.236 782(69)	−2.278 293(122)	0.928 383(204)
$D_K \times 10^3$	6.987 419(74)	7.152 212(162)	6.900 814(118)	7.000 837(112)	7.059 185(131)	−0.843 033(280)
$\delta_J \times 10^3$	0.394 369 37(157)	0.394 297 8(72)	0.395 681 0(74)	0.393 310 8(91)	0.391 990 6(149)	0.355 380 6(297)
$\delta_K \times 10^3$	1.248 369(34)	1.314 005(70)	1.249 262(70)	1.238 510(90)	1.376 406(135)	2.361 658(274)
$\Phi_J \times 10^9$	0.417 539(303)	0.400 72(107)	0.426 68(98)	0.401 95(122)	0.286 17(245)	8.088 5(53)
$\Phi_{JJK} \times 10^6$	0.005 663 3(62)	0.006 384 2(113)	0.005 397 9(114)	0.005 591 0(141)	0.007 450 8(283)	−0.100 479(59)
$\Phi_{JKK} \times 10^6$	−0.041 565 8(193)	−0.044 976 8(312)	−0.041 310 9(312)	−0.040 152(42)	−0.048 894(82)	−0.045 983(174)
$\Phi_K \times 10^6$	0.059 657(33)	0.064 268(67)	0.059 133(43)	0.058 436(46)	0.064 680(59)	0.016 567(126)
$\phi_J \times 10^9$	0.222 193(143)	0.221 27(55)	0.218 79(53)	0.215 72(69)	0.185 37(128)	4.019 04(284)
$\phi_{JK} \times 10^9$	1.201 0(40)	1.404 6(86)	1.109 9(86)	1.108 3(112)	3.257 8(204)	−18.391(45)
$\phi_K \times 10^6$	0.017 002 9(200)	0.019 180(33)	0.017 341 9(311)	0.015 719(48)	0.023 082(96)	−0.044 376(200)
$L_K \times 10^{12}$	−0.180 6(43)	−0.239 9(77)	[−0.180 6]	[−0.180 6]		
N	9 363	5 172	7 760	9 082	5 442	2 091
Standard deviation	MW: 0.100 017 MHz/far-IR: 0.000 12 cm^{-1}/unitless: 0.993 13					

	[35, 37]					
	GS	ν_4	ν_6	ν_3	ν_5	ν_2
ν			8 455 900.87(41)	10 316 192.76(35)	13 732 558.936(216)	14 940 637.49(33)
ν (cm^{-1})			282.058 492(13)	344.111 150(11)	458.068 859 6(72)	498.366 023(11)
A	5 044.367 089(127)		5 032.282 14(169)	5 036.686 6(58)	5 030.390 3(118)	5 042.574 8(262)
B	2 748.942 296(60)		2 752.440 67(48)	2 742.964 17(123)	2 736.642 37(248)	2 749.443 0(64)
C	1 918.657 984(64)		1 918.703 17(32)	1 916.957 178(295)	1 910.689 110(124)	1 917.742 719(258)
$D_J \times 10^3$	1.072 545 9(100)		1.135 913(37)	1.092 708(243)	1.113 03(128)	0.805 9(42)
$D_{JK} \times 10^3$	−2.133 234(44)		−2.194 09(33)	−2.242 6(39)	−4.501(45)	2.417(82)
$D_K \times 10^3$	6.868 634(127)		6.824 13(148)	6.973 5(206)	13.476(129)	2.053(307)
$\delta_J \times 10^3$	0.373 416 1(46)		0.396 376 4(230)	0.393 767(126)	0.399 34(64)	0.234 12(211)
$\delta_K \times 10^3$	1.230 534(47)		1.255 594(263)	1.241 02(207)	0.455 7(179)	2.162(39)
$\Phi_J \times 10^9$	0.382 34(61)		[0.382 34]	[0.382 34]		
$\Phi_{JJK} \times 10^6$	0.005 410 6(77)		[0.005 410 6]	[0.005 410 6]		
$\Phi_{JKK} \times 10^6$	−0.039 788 8(230)		[−0.039 788 8]	[−0.039 788 8]		
$\Phi_K \times 10^6$	0.058 070(54)		[0.058 070]	[0.058 070]		
$\phi_J \times 10^9$	0.203 364(314)		[0.203 364]	[0.203 364]		
$\phi_{JK} \times 10^9$	1.167 7(55)		[1.167 7]	[1.167 7]		
$\phi_K \times 10^6$	0.016 741 3(243)		[0.016 741 3]	[0.016 741 3]		
$L_K \times 10^{12}$	−0.221 6(64)		[−0.221 6]	[−0.221 6]		
N	7 770		2 498	2 604	1 532	854
Standard deviation	MW: 0.090 167 MHz/far-IR: 0.000 292 cm^{-1}/unitless: 1.035 56					

We have chosen this method of calculation since it can determine rotational constants, and harmonic and anharmonic vibrational frequencies for medium-sized molecules with acceptable accuracy and with reasonable computational cost using computing clusters that are now commonly accessible. A better quantitative agreement is obtained (at much higher computational cost) by using coupled cluster techniques such as the coupled-cluster singles and doubles (CCSD) level augmented by a perturbative treatment of triple excitations, CCSD(T).[39] Therefore the high-resolution spectroscopic study of $SOCl_2$ presented here was complemented with quantum-chemical calculations using the CCSD(T) method.

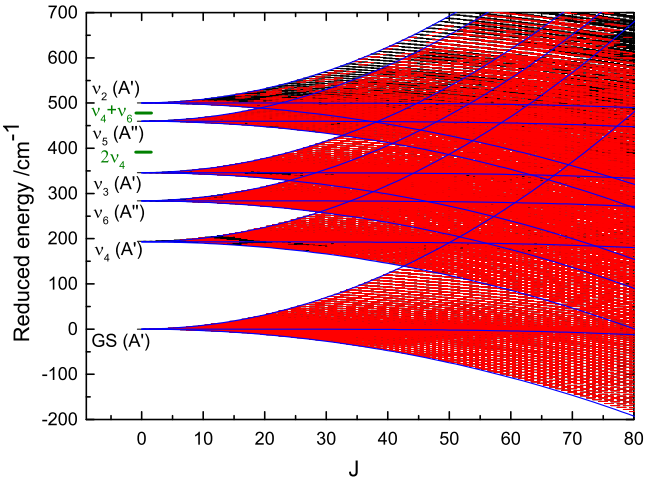

FIG. 7. Calculated rovibrational energies for the vibrational ground state, the $\nu_2, \nu_3, \nu_4, \nu_5$, and ν_6 bands of [35, 35] up to $J = 80$. To improve visibility, we did not plot the rovibrational energies E but the reduced energies $E - B^{(v)}J(J+1)$. The red levels belong to assigned experimental transitions. Each band is computed with its own effective rotational constant $B^{(v)}$. The curves represent the energy of the classical stationary axes of rotation (relative equilibria). The two green levels represent the energy level of the $\nu_4 + \nu_6$ (474.017 cm^{-1}) combination band and the 2 ν_4 (387.023 cm^{-1}) overtone band calculated at the anharmonic MP2/6-311++G(3df,3pd) level of theory.[7]

All calculations were performed using the CFOUR suite of programs.[40] See Ref. 4 for more details on the calculations and Ref. 41 for the general strategies used.

The rotation-vibration interaction constants, resultant rotational constants, and harmonic and anharmonic vibrational frequencies at the CCSD(T) level are summarized in the supplementary material. The rotational constants of the $v_2 = 1$ and $v_5 = 1$ states computed with this method have been compared with those determined from EAs for the [35, 35] and [35, 37] isotopologues. In the case of $v_5 = 1$, the rotational constants determined by EAs are closer to the final experimental values compared to the CCSD(T) constants. As example, for the A rotational constant of $v_5 = 1$, the relative accuracy δ of EAs is one order of magnitude better than that of the coupled cluster calculations. This is not the case for $v_2 = 1$, where the CCSD(T) computations and the EAs procedure provide the same level of accuracy for the prediction of the rotational constants. While the prediction of rotational constants by the CCSD(T) method can be considered more or less competitive with their determination by the EAs, the most advanced quantum chemistry methods do not compete yet with the EAs determination of the vibrational band centers. Indeed, when we confront the two methods for the predictions of the ν_2 and ν_5 vibrational band centers for both isotopologues, the EAs relative accuracies are improved by three orders of magnitude compared to the CCSD(T) anharmonic force field calculations.

VII. CONCLUSIONS

The $SOCl_2$ high-resolution spectrum of the ν_2 and ν_5 bands measured in the far-IR domain at the SOLEIL synchrotron facility has been assigned in spite of the large density of lines and the presence of the ν_2 fundamental band of SO_2. Our strategy consisted in using an evolutionary algorithm to adjust first the rotational constants and vibrational band centers of the main isotopologues by maximizing the overlap between the experimental and the calculated spectra. The accuracy of these parameters was good enough for them to be used as starting values in the traditional line-by-line spectroscopic analysis. In addition to saving time in the analysis, these two approaches are complementary and become very powerful for the analysis of very congested spectra. The obtained parameters for the $v_2 = 1$ and $v_5 = 1$ vibrational states of the [35, 35] have been refined in the analysis of a pure rotational submillimeter spectrum. The pure rotational transitions in the $v_4 = 1$ vibrational state inactive in the far-IR have been assigned in the same submillimeter spectrum. A global fit using the rotational and rovibrational assignments has been performed, revealing no major resonance in the energy levels of the main isotopologue. In addition to the global analysis of the fundamental low-lying vibrational modes of $SOCl_2$, this article highlights a particularly efficient method to untangle a difficult assignment in very dense high resolution-rovibrational spectra. Even with the CCSD(T) method, the predicted anharmonic vibrational band centers cannot reach the level of accuracy obtained by the EAs procedure. The relative accuracies of the EAs rotational constants in the $v_2 = 1$ and $v_5 = 1$ vibrational states for [35, 35] and [35, 37] isotopologues are competitive with those obtained with the highest level of theory of quantum chemical methods. Finally, the analysis of the ν_1 symmetric (A') mode which corresponds to the SO stretching mode remains to be performed. This mode calculated at 1259 cm^{-1} in a CCSD(T)/cc-pV(T+d)Z computation of anharmonic frequencies belongs to the mid-IR region. A step in the direction of a global knowledge of the IR spectrum, including the overtone and combination bands, could be realized with the construction of a six-dimensional potential energy surface of $SOCl_2$.

SUPPLEMENTARY MATERIAL

See supplementary material for the results of CCSD(T) calculations. The rotation-vibration interaction constants α_i and the resulting *ab initio* rotational constants for each $v_i = 1$ excited states of $^{32}S^{16}O^{35}Cl_2$ and $^{32}S^{16}O^{35}Cl^{37}Cl$ isotopologues are given in the first table. *Ab initio* harmonic and anharmonic vibrational frequencies and intensities are listed in the second table.

ACKNOWLEDGMENTS

We thank the Ph.D. financial supports of Anthony Roucou, i.e., the region Haut-de-France and the French Délégation Générale pour l'Armement. A. Roucou was awarded an EOLE fellowship (excellence scholarship of the Franco-Dutch network) which permitted him to visit W. L. Meerts at Radboud Universiteit, Nijmegen, The Netherlands. Some of the computations presented in this paper were carried out using the CALCULCO computing platform, supported by SCoSI/ULCO (Service Commun du Système d'Information de l'Université du Littoral Côte d'Opale). The authors are grateful to SOLEIL for beamtime allocation on the AILES beamline under

Proposal No. 20141064; we thank Pascale Roy, Olivier Pirali, and the AILES team. The submillimeter work is supported by the French Délégation Générale pour l'Armement (Projet de Recherche Exploratoire et Innovation No. 06.34.037). S.T. acknowledges support by the Deutsche Forschungsgemeinschaft (DFG) through Grant No. SCHL 341/15-1 and the Regional Computing Center of the Universität zu Köln for computing time on the DFG-funded High Performance Computing system CHEOPS.

[1]T. J. Johnson, R. S. Disselkamp, Y.-F. Su, R. J. Fellows, M. L. Alexander, and C. J. Driver, J. Phys. Chem. A **107**, 6183 (2003).
[2]L. A. Corio, T. S. Ziolkowski, J. K. Walker, W. B. Jones, B. William, and T. Belisle, in *Proceedings of the Air and Waste Management Association's Annual Meeting & Exhibition* (A&WMA, 1996), p. 16.
[3]Y. L. Chang and M. S. Strano, J. Am. Chem. Soc. **130**, 1766 (2008).
[4]M.-A. Martin-Drumel, A. Roucou, G. G. Brown, S. Thorwirth, O. Pirali, G. Mouret, F. Hindle, M. C. McCarthy, and A. Cuisset, J. Chem. Phys. **144**, 084305 (2016).
[5]A. P. Uthman, P. J. Demlein, T. D. Allston, M. C. Withiam, M. J. McClements, and G. A. Takacs, J. Phys. Chem. **82**, 2252 (1978).
[6]D. E. Martz and R. T. Lagemann, J. Chem. Phys. **22**, 1193 (1954).
[7]M.-A. Martin-Drumel, G. Mouret, O. Pirali, and A. Cuisset, J. Mol. Spectrosc. **315**, 30 (2015).
[8]W. L. Meerts, M. Schmitt, and G. C. Groenenboom, Can. J. Chem. **82**, 804 (2004).
[9]W. L. Meerts and M. Schmitt, Int. Rev. Phys. Chem. **25**, 353 (2006).
[10]J. A. Hageman, R. Wehrens, R. de Gelder, W. L. Meerts, and L. M. C. Buydens, J. Chem. Phys. **113**, 7955 (2000).
[11]J. Wilke, M. Wilke, W. L. Meerts, and M. Schmitt, J. Chem. Phys. **144**, 044201 (2016).
[12]G. M. P. Just, P. Rupper, T. A. Miller, and W. L. Meerts, Phys. Chem. Chem. Phys. **12**, 4773 (2010).
[13]J. van Wijngaarden, D. Desmond, and W. L. Meerts, J. Mol. Spectrosc. **315**, 107 (2015).
[14]J.-B. Brubach, L. Manceron, M. Rouzieres, O. Pirali, D. Balcon, F. K. Tchana, V. Boudon, M. Tudorie, T. Huet, A. Cuisset *et al.*, AIP Conf. Proc. **1214**, 81–84 (2010).
[15]F. W. Loomis and R. W. Wood, Phys. Rev. **32**, 223 (1928).
[16]I. Merke and H. Dreizler, Z. Naturforsch. A **47**, 1150 (1992).
[17]A. Dubrulle, D. Boucher, and C. R. Hebd, Séances Acad. Sci. Sér. B **274**, 1426 (1972).
[18]H. S. P. Müller and M. C. L. Gerry, J. Chem. Soc., Faraday Trans. **90**, 3473 (1994).
[19]J. Burie, J.-L. Destombes, A. Dubrulle, G. Journel, and C. R. Hebd, Séances Acad. Sci. Sér. B **267**, 48 (1968).
[20]G. Journel, Ph.D. thesis, University of Lille, 1969.
[21]D. Jacquemart, L. Gomez, N. Lacome, J.-Y. Mandin, O. Pirali, and P. Roy, J. Quant. Spectrosc. Radiat. Transfer **111**, 1223 (2010).
[22]Sigma-Aldrich, Thionyl chloride, reagent grade, 97%, reference 320536, 2016.
[23]W. J. Lafferty, J.-M. Flaud, R. L. Sams, and E. H. Abib Ngom, J. Mol. Spectrosc. **252**, 72 (2008).
[24]V.-M. Horneman, R. Anttila, S. Alanko, and J. Pietilä, J. Mol. Spectrosc. **234**, 238 (2005).
[25]F. Matsushima, H. Odashima, T. Iwasaki, S. Tsunekawa, and K. Takagi, J. Mol. Struct. **352**, 371 (1995).
[26]N. Hansen and A. Ostermeier, Evol. Comput. **9**, 159 (2001).
[27]N. Hansen and S. Kern, "Evaluating the CMA evolution strategy on multimodal test functions," in *Proceedings of Parallel Problem Solving from Nature–PPSN VIII: 8th International Conference, Birmingham, UK, September 18-22, 2004*, Lecture Notes in Computer Science, edited by X. Yao, E. K. Burke, J. A. Lozano, J. Smith, J. J. Merelo-Guervós, J. A. Bullinaria, J. E. Rowe, P. Tiňo, A. Kabán, and H.-P. Schwefel (Springer, Berlin, Heidelberg, 2004), Vol. 3242, pp. 282–291.
[28]M. Schmitt and W. L. Meerts, "Rotationally resolved electronic spectroscopy and automatic assignment techniques using evolutionary algorithms," in *Handbook of High-Resolution Spectroscopy* (John Wiley & Sons, Chichester, United Kingdom, 2011), pp. 1345–1371.
[29]We ran the EA program parallel on 20 cores of Intel Xeon E5-2430L processors at 2.4 GHz. The time mentioned is the wall-clock time.
[30]H. M. Pickett, J. Mol. Spectrosc. **148**, 371 (1991).
[31]W. Łodyga, M. Kreglewski, P. Pracna, and Š. Urban, J. Mol. Spectrosc. **243**, 182 (2007).
[32]Documentation for SPFIT and SPCAT, https://spec.jpl.nasa.gov/ftp/pub/calpgm/spinv.pdf, section Format of the .par file and .var files, FRAC keyword. See also http://www.ifpan.edu.pl/~kisiel/asym/pickett/crib.htm#frac.
[33]G. Mouret, M. Guinet, A. Cuisset, L. Croizé, S. Eliet, R. Bocquet, and F. Hindle, IEEE Sens. J. **13**, 133 (2013).
[34]Z. Kisiel, E. Białkowska-Jaworska, and L. Pszczółkowski, J. Chem. Phys. **109**, 10263 (1998).
[35]Z. Kisiel, E. Białkowska-Jaworska, and L. Pszczółkowski, J. Mol. Spectrosc. **199**, 5 (2000).
[36]W. G. Harter, Comput. Phys. Rep. **8**, 319 (1988).
[37]D. A. Sadovskií and B. I. Zhilinskií, Mol. Phys. **65**, 109 (1988).
[38]G. Dhont, D. Sadovskií, B. Zhilinskií, and V. Boudon, J. Mol. Spectrosc. **201**, 95 (2000).
[39]K. Raghavachari, G. W. Trucks, J. A. Pople, and M. Head-Gordon, Chem. Phys. Lett. **157**, 479 (1989).
[40]CFOUR, Coupled-Cluster techniques for Computational Chemistry, a quantum-chemical program package by J. F. Stanton, J. Gauss, M. E. Harding, and P. G. Szalay with contributions from A. A. Auer, R. J. Bartlett, U. Benedikt, C. Berger, D. E. Bernholdt, Y. J. Bomble, L. Cheng, O. Christiansen, F. Engel, R. Faber, M. Heckert, O. Heun, C. Huber, T.-C. Jagau, D. Jonsson, J. Juslius, K. Klein, W. J. Lauderdale, F. Lipparini, D. A. Matthews, T. Metzroth, L. A. Mck, D. P. O'Neill, D. R. Price, E. Prochnow, C. Puzzarini, K. Ruud, F. Schiffmann, W. Schwalbach, C. Simmons, S. Stopkowicz, A. Tajti, J. Vzquez, F. Wang, and J. D. Watts and the integral packages MOLECULE (J. Almlfand P. R. Taylor), PROPS (P. R. Taylor), ABACUS (T. Helgaker, H. J. A. Jensen, P. Jrgensen, and J. Olsen), and ECP routines by A. V. Mitin and C. van Wllen. For the current version, see http://www.cfour.de.
[41]C. Puzzarini, J. F. Stanton, and J. Gauss, Int. Rev. Phys. Chem. **29**, 273 (2010).